Experimental and Numerical Study of Bonded Sand/Air Two-Phase Flow in PUA Process

Sayavur I. Bakhtiyarov
Auburn University, AL

Ruel A. Overfelt
Auburn University, AL

ABSTRACT

The results of an experimental study and numerical simulations of resin bonded sand/air flow in a square corebox with an H-shape insertion and passage between upper and lower pockets of the pattern are presented. A computer controlled electronic system was designed and built to measure pressures and flow rates inside the corebox during mold filling, gassing and purging cycles of Phenolic Urethane Amine (*PUA*) process. Contour maps of the pressure distributions inside the corebox were created based on barometric measurements. A good agreement between experimental results and numerical simulations was found.

INTRODUCTION

To optimize the structure and properties of cast metals a variety of casting techniques has evolved over the past few decades. Cold box or Phenolic Urethane Amine (PUA) process has many advantages in terms of productivity, reduced energy consumption, tolerance and high quality of the mold. This particular processing technique involves room-temperature curing of a resin-bonded sand core accelerated by a gas catalyst passed through the sand-binder mixture. Chemical binders provide a flowability to the sand mix that easily is blown into complicated patterns. In principle, the process possesses relatively fast *Sand Blowing, Gassing, Purging,* and *Stripping* cycles, which are mainly affected by sand properties (density, grain size and size distribution, shape, moisture content, close-pack volume fraction, etc.), type and amount of binders (ratios for two or more part binders system), tooling design (blow tubes, sand magazine, input and exhaust piping and manifolds, vents, exhaust ports, core box, etc.), gassing and purging performance (gas type, pressure, time, temperature, flowrate, etc.).

Recently, we investigated the flow dynamics of phenolic-urethane-amine process in a core box of an inverted "*U*" configuration experimentally using a commercial core shooter (Bakhtiyarov and Overfelt, 1998b). The effects of reduction in area of the vents were evaluated by manual reduction of the active vent areas. In addition, experimental data on the pressure drop and friction factor for the vents were obtained as a function of the amounts of sand deposited in the vent area. The experimental data were compared with the predictions of the Blake-Kozeny and Ergun porous flow equations and good agreement was found.

Special experiments were conducted to measure the variation of the pressure with the amount of resin bonded sand bed deposited in cylindrical corebox (Bakhtiyarov and Overfelt, 2001). A non-linear relationship between pressure and air flowrate was established. Due to the sand compaction, the pressure increased with increasing the air flowrate for resin-bonded sands. It was shown that the pressure drop also increases non-linearly with amount of deposited resin bonded sand. Moreover, at certain values of the air flowrate (~ 250 cm^3/s) a significant increase in pressure drop was observed for resin-bonded sand, which was attributed to the complex rheological behavior of the test material. The plasticity of the sand+binders mixture was characterized by a shear yield stress, which provides some "resistance" to the system against compaction. Significant differences in pressure were observed in the hopper, blowtube, and inside the corebox. These differences were related to the cross section area changes and transition of the system from packed bed to fluidized bed. A good agreement was found between the numerically simulated and experimentally measured values of pressure along the vertical symmetry axis of the corebox.

In this paper we present the results of numerical predictions and experimental measurements of pressure variations and flow rate during bonded sand/air two-phase system flow in core molding process. A square corebox with H-shape insertion and passage between upper and lower pockets of the pattern was used in this study.

CFD MODELING OF SAND CORE SHOOTING PROCESS

CFD modeling of sand core shooting process was based on a two-fluid flow approach. The following governing equations were used in our computations.

Continuity equations:

$$\frac{\partial \varepsilon_g}{\partial t} + \nabla \cdot \left(\varepsilon_g \upsilon_g\right) = 0\,, \qquad \text{Equation 1}$$

$$\frac{\partial \varepsilon_s}{\partial t} + \nabla \cdot \left(\varepsilon_s \upsilon_s\right) = 0\,. \qquad \text{Equation 2}$$

Momentum equations:

$$\rho_g\left[\frac{\partial \upsilon_g}{\partial t} + \upsilon_g \nabla \upsilon_g\right] = \nabla \cdot \tilde{\tau}_g - \nabla P - \frac{\beta}{\varepsilon_g}\left(\upsilon_g - \upsilon_s\right) + \rho_g g\,, \qquad \text{Equation 3}$$

$$\rho_s \varepsilon_s\left[\frac{\partial \upsilon_s}{\partial t} + \upsilon_s \nabla \upsilon_s\right] - \rho_g \varepsilon_s\left[\frac{\partial \upsilon_g}{\partial t} + \upsilon_g \nabla \upsilon_g\right] = \nabla \cdot \tilde{\tau}_s - \nabla P_s + \frac{\beta}{\varepsilon_g}\left(\upsilon_g - \upsilon_s\right) + \varepsilon_s\left(\rho_s - \rho_g\right) \qquad \text{Equation 4}$$

where

$$\tilde{\tau}_i = 2 \quad \mu_i \, \tilde{D}_i + \left(\lambda_i - \frac{2}{3}\mu_i\right) tr\left(\tilde{D}_i\right)\tilde{I}\,, \qquad \text{Equation 5}$$

$$\tilde{D}_i = \frac{1}{2}\left(\nabla \upsilon_i + \left(\nabla \upsilon_i\right)^T\right). \qquad \text{Equation 6}$$

If the momentum equations are considered in terms of the resulting coefficients C_{ij}, and nodal velocities u_j, then the pressure gradients may be determined from:

$$C_{ii}\, u_i = -\sum C_{ij}\, u_i + \varepsilon_i - \int n_i \, \frac{\partial p}{\partial x} dv\,, \qquad \text{Equation 7}$$

$$u_i = \hat{u} - \frac{1}{C_{ii}} \int n_i \, \frac{\partial p}{\partial x}\, dv = \hat{u} - K_i \frac{\partial p}{\partial x}\,, \qquad \text{Equation 8}$$

$$\hat{u} = \frac{-\sum C_{ij} + \varepsilon_i}{C_{ii}}, \quad K_i = \frac{\int n_i \, dv}{C_{ii}}, \qquad \text{Equation 9}$$

where ε is volume fraction; υ is velocity; ρ is density; τ is viscous stress tensor; P is pressure; β is drag coefficient; $\tilde{D}$ is strain tensor rate; μ is viscosity; K is conductivity matrix; n is an interpolating function; subscripts g and s refer to gas and solid phases, respectively.

Earlier we investigated the rheological properties of resin bonded sand/air mixture (Bakhtiyarov and Overfelt, 1998b) using both capillary and rotational viscometers. It was demonstrated that resin bonded sand/air mixture exhibits strong non-Newtonian, shear thinning behavior over wide ranges of shear rates. Therefore in our simulations we used Ostwald model as a rheological equation to describe resin bonded sand/air flow:

$$\eta = \kappa\, \dot{\gamma}^{n-1} , \qquad \text{Equation 10}$$

where κ is a measure of the consistency of the system, n is a measure of the degree of non-Newtonian behavior.

Typical results of 2-dimensional transient CFD simulations are presented in Figures 1-11. As seen from these figures, the actual mold filling cycle takes only 0.2 sec. The results of 3-dimensional CFD simulations showed that a variation of the velocity component in the transverse direction is negligible compared to other two velocity components. As an example, in Figure 12 we present the 3-dimensional CFD simulation results for mold filling cycle at $t = 0.14$ sec.

EXPERIMENTAL APPARATUS AND PROCEDURE

Silica sand was used in our experiments. As a cold box binder system we used ISOCURE LF-305/904 G system. This system consists of an ISOCURE Part I LF-305 phenol-formaldehyde binder and an ISOCURE Part II 52-904 GR binder containing a polymeric isocyanate with solvents and additives. The reaction between Parts I and II results in the formation of phenolic urethane polymer. According to industry procedures and the manufacturer's instructions, in our experiments we used the composition at a 55/45 ratio of ISOCURE Part I binder to ISOCURE Part II binder components. Increasing the amount of the Part I decreases the humidity resistance of the core and benchlife of mixed sand. Increasing the amount of the Part II increases the cost and shakeout time of the core product. Recently we experimentally investigated the rheological and thermal properties of the phenolic resin and polymeric isocyanate (ISOCURE© and TECHNIKURE®), and their blends (Bakhtiyarov and Overfelt, 1997a, 1997b, 1998a). We determined that although both binders are Newtonian liquids, their blends exhibit non-Newtonian shear thinning fluid flow behavior and elasticity. The dynamic viscosity of the blends increases both with time and with increasing the ISOCURE Part I LF-305 content, and may reach comparatively large values at large values of either parameter. The increase in viscosity of blends is explained as the result of the rubbery nature of the phenolic urethane polymer produced as a product of reaction between Parts I and II. Due to degradation effects at high shear rates, the viscosity of blends decreases. At fixed shear rates we observed a temperature rise during the mixing of binders. Following the manufacturer's instructions the total binder level was 1.5% based on sand weight. Before being blown into the pattern, sand was coated with the binders. The bulk density of the coated sand was 1.426 g/cm^3. For gassing we used liquid triethylamine (Catalyst 700), which was vaporized during curing.

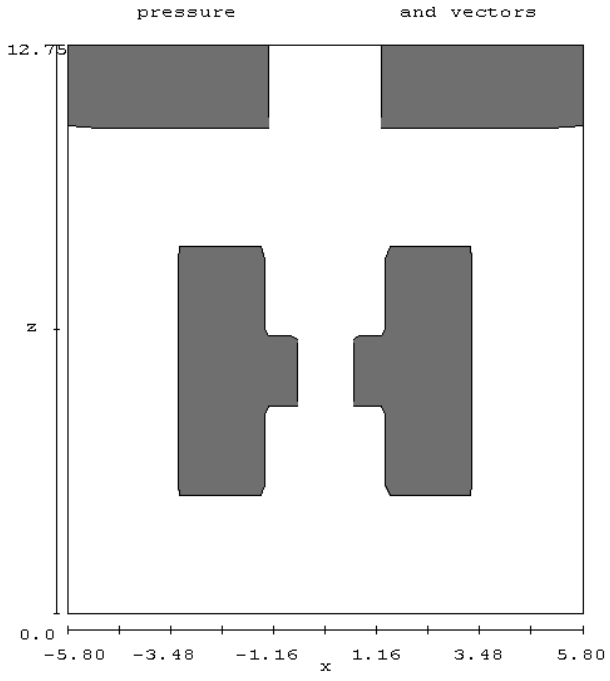

Figure 1. CFD simulations of mold filling process: $t = 0.00$ s.

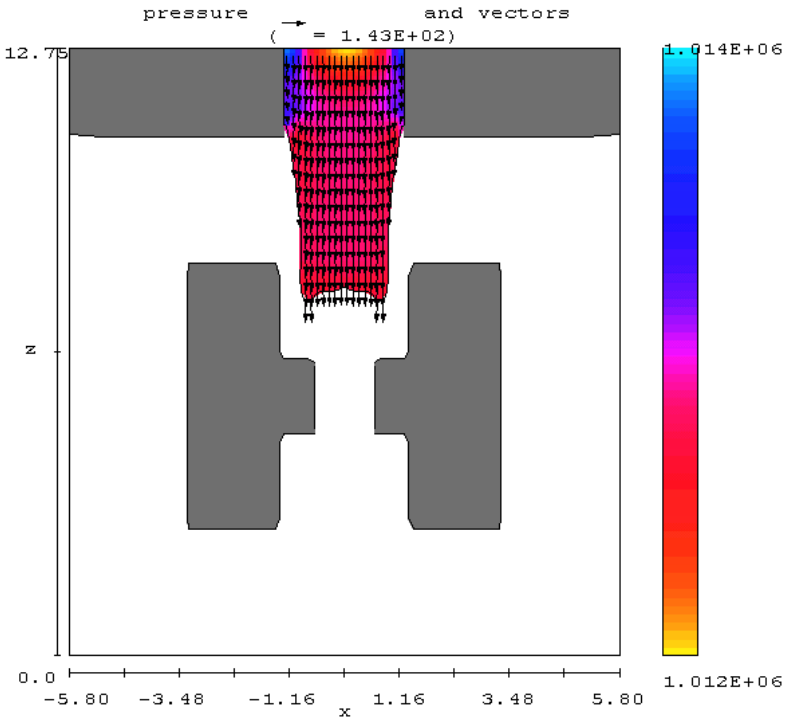

Figure 2. CFD simulations of mold filling process: t = 0.02 s.

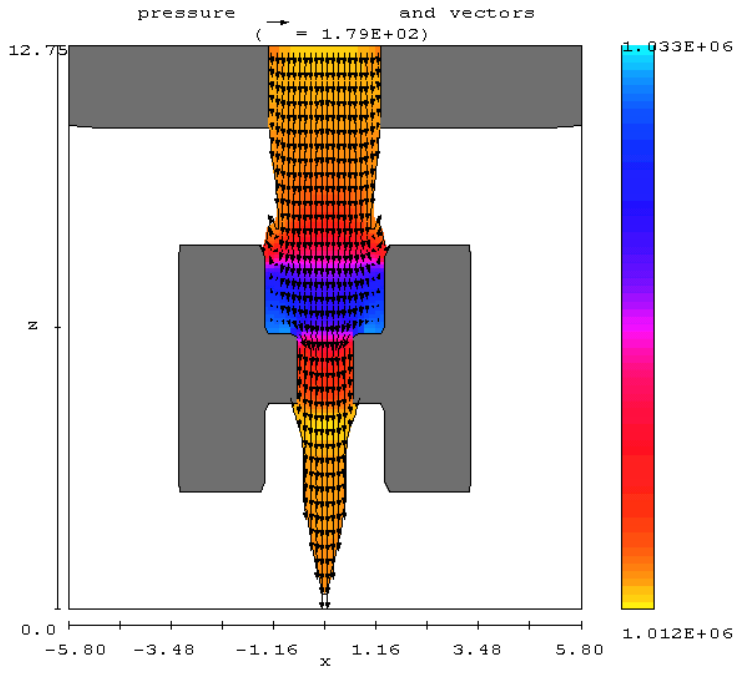

Figure 3. CFD simulations of mold filling process: t = 0.04 s.

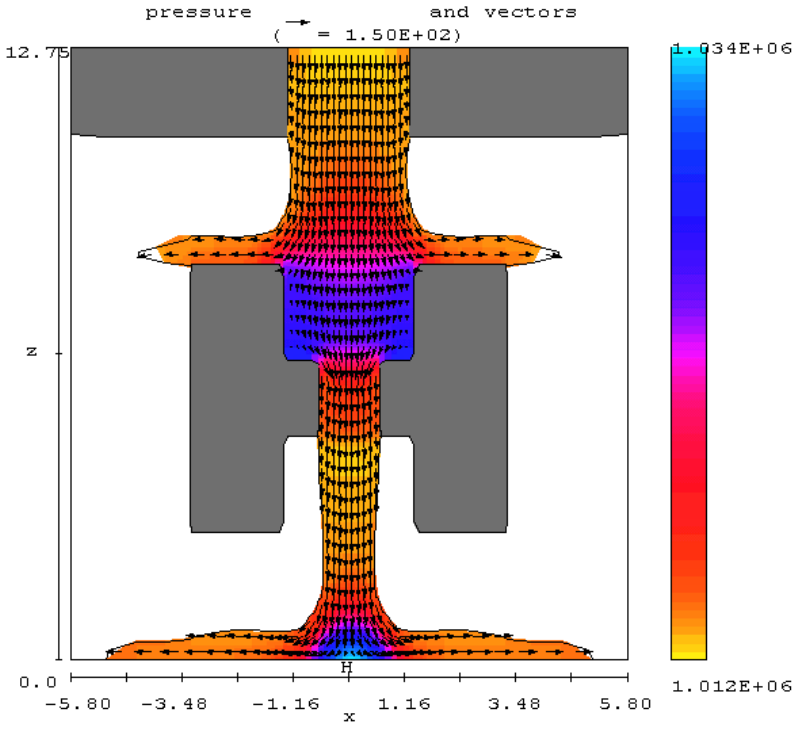

Figure 4. CFD simulations of mold filling process: t = 0.06 s.

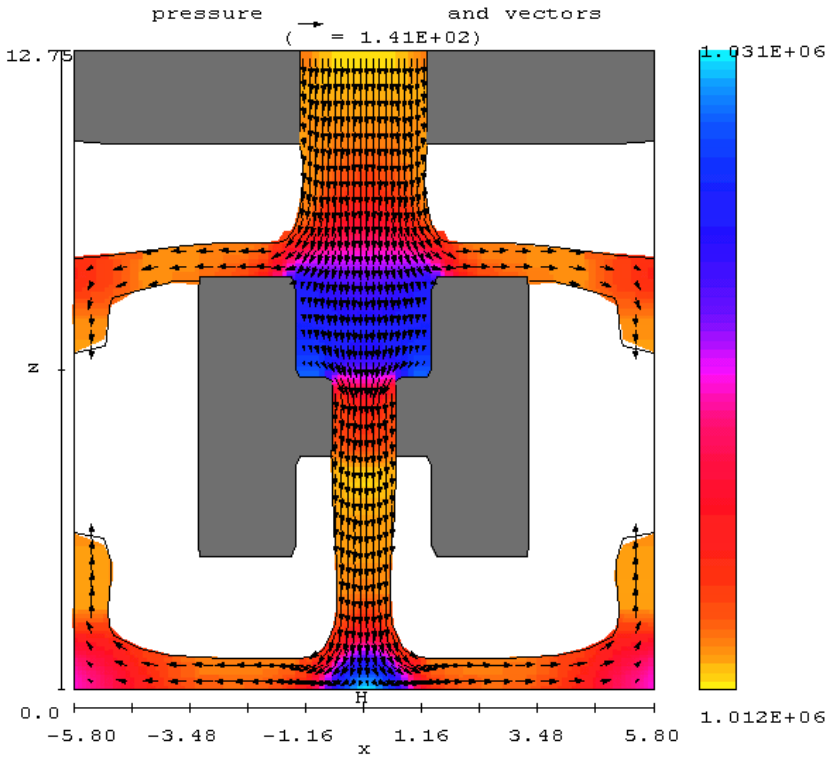

Figure 5. CFD simulations of mold filling process: t = 0.08 s.

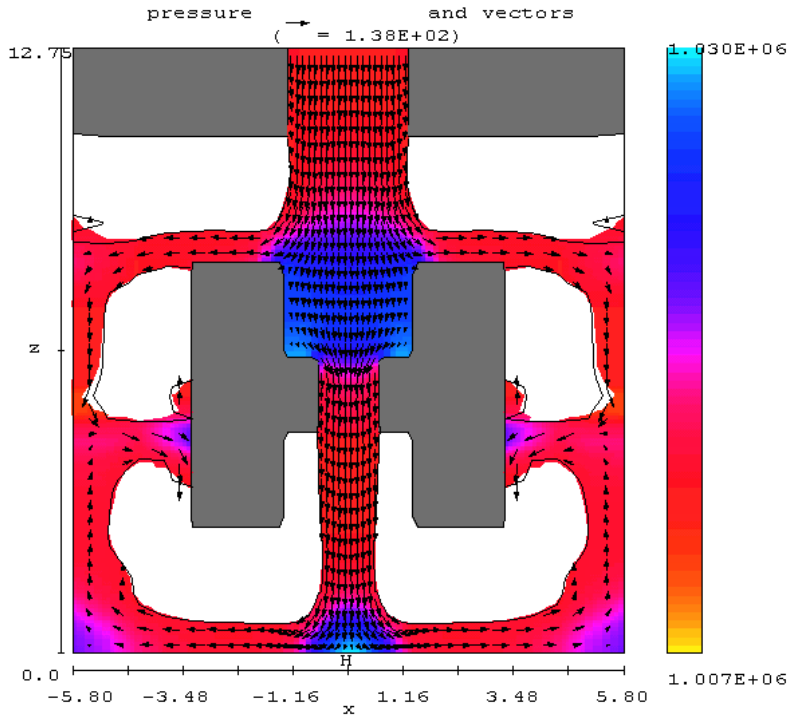

Figure 6. CFD simulations of mold filling process: $t = 0.10$ s.

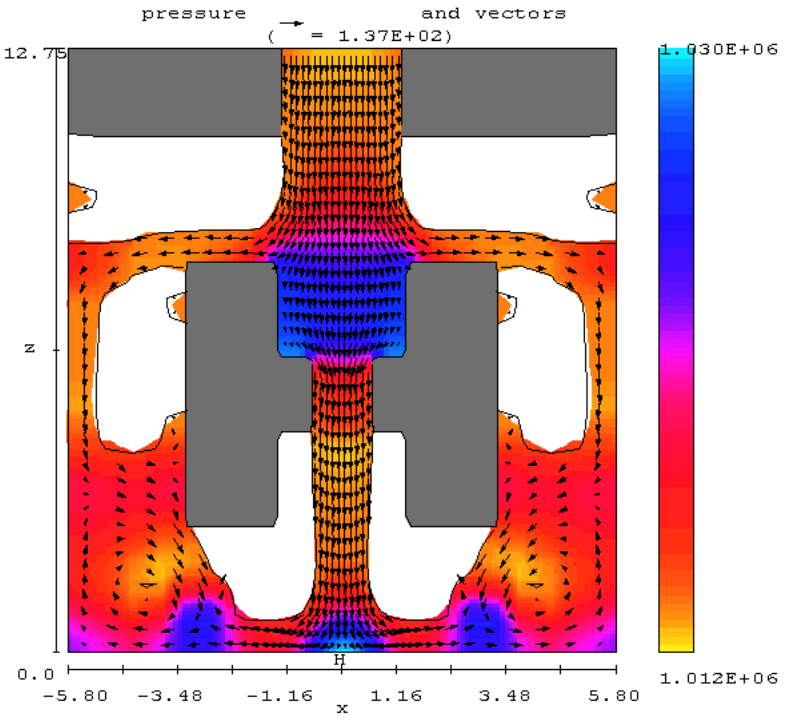

Figure 7. CFD simulations of mold filling process: $t = 0.12$ s.

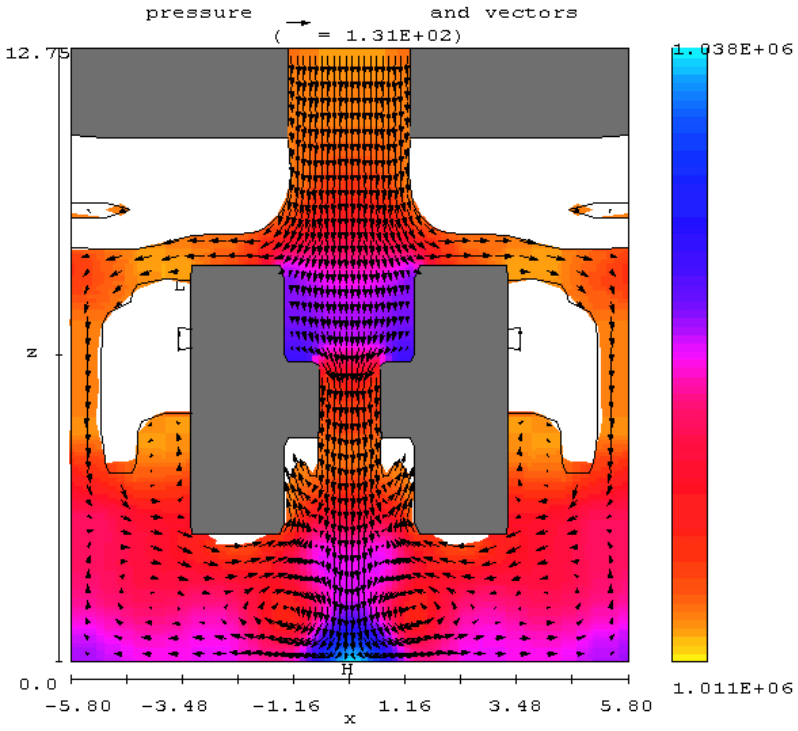

Figure 8. CFD simulations of mold filling process: $t = 0.14$ s.

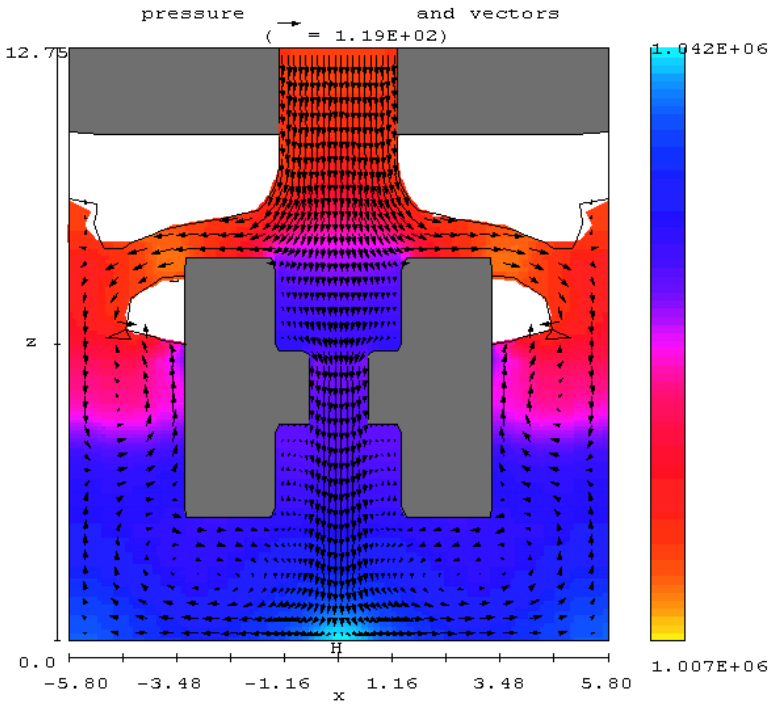

Figure 9. CFD simulations of mold filling process: $t = 0.16$ s.

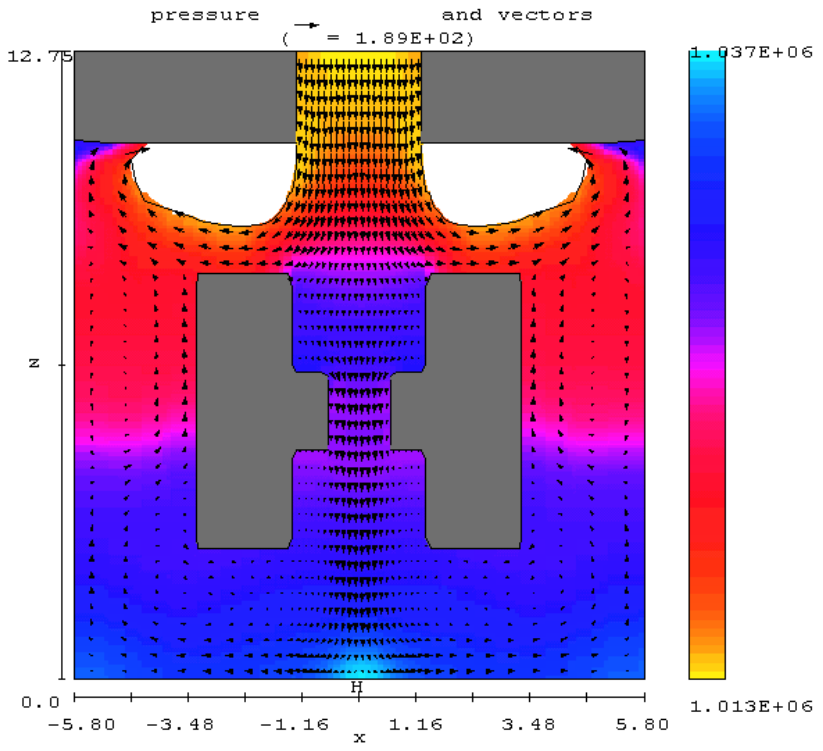

Figure 10. CFD simulations of mold filling process: $t = 0.18$ s.

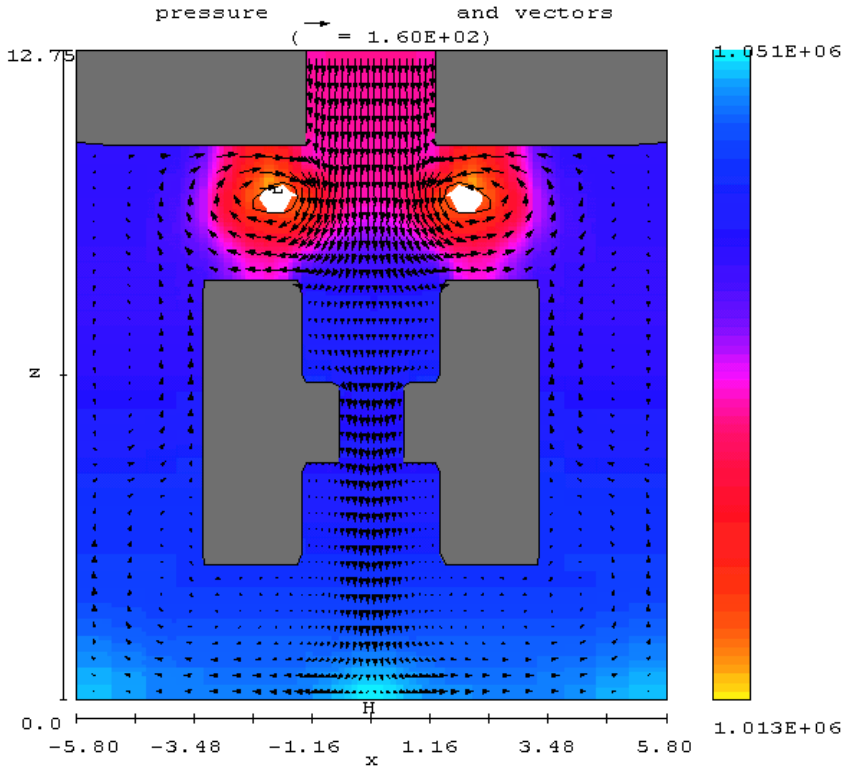

Figure 11. CFD simulations of mold filling process: $t = 0.20$ s.

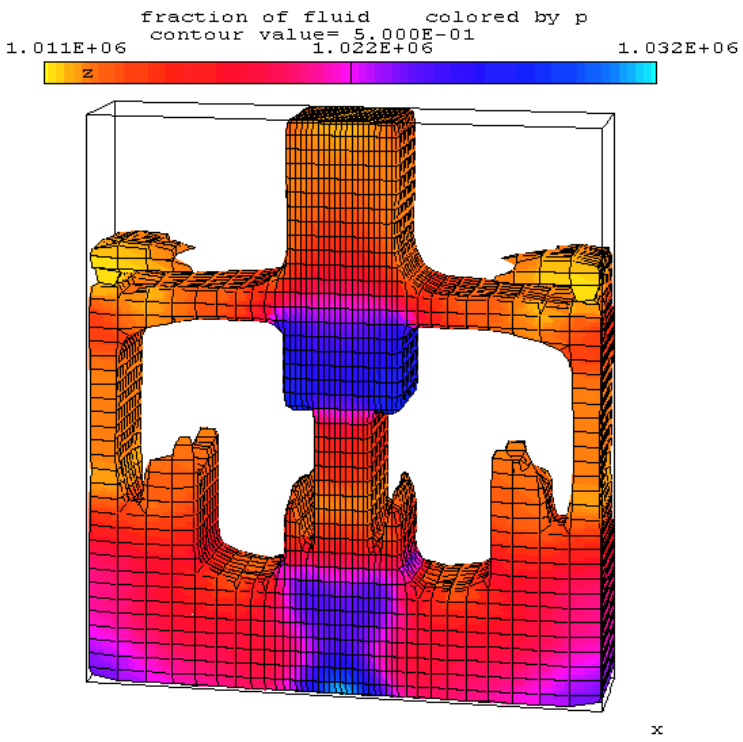

Figure 12. 3D CFD simulations of mold filling process: t = 0.14 s.

A special pressure measurement system was designed and built with safety and portability requirements of the foundry environment. All sensor electronics were housed in a special briefcase and were connected to a computer controlled data acquisition system through PC-LPM-16/DAQCard-700. Up to 14 piezoresistive absolute pressure sensors PX72-100V suitable for PC board mounting (linearity: ± 0.5% FS, repeatability: ± 0.3% FS, operating temperature range: -15 to 85^0 C) were used in a single experiment. These are stable, high performance micromachined silicon diaphragm sensors without temperature compensation for operating ranges of 0 to 690 kPa. The sensors exhibit a response time of 0.1 s and were operated from a constant current excitation supply. To prevent penetration of sand and dust particles into the measurement system, porous metallic element brass pressure snubbers were mounted on each pressure tap. The snubbers also protect transducers and other delicate line installations from shock damage caused by pressure pulsation, surges, and fluctuations. The snubbers contain a Type 316 stainless steel porous disc (porosity designation D and rating 40-45 μm). After each experiment all snubbers were brushed and washed in acetone. Special experiments were run to determine the effect of the snubbers on measured pressure values. The test results for pressure transducer # 14 are shown in Figure 13. As seen from this figure, the influence of the snubber on measured pressure values is negligible (less than 1%).

The calibration results showed that the output voltage (V_{out}) of pressure transducers increases linearly with increasing pressure. This relationship can be expressed as

$$P = \alpha V_{out} - \beta \qquad \text{Equation 11}$$

where α and β are calibration coefficients of the pressure sensors. These coefficients were determined experimentally for each pressure sensor system (sensors, hoses, connectors, etc.) and results are presented in Table 1.

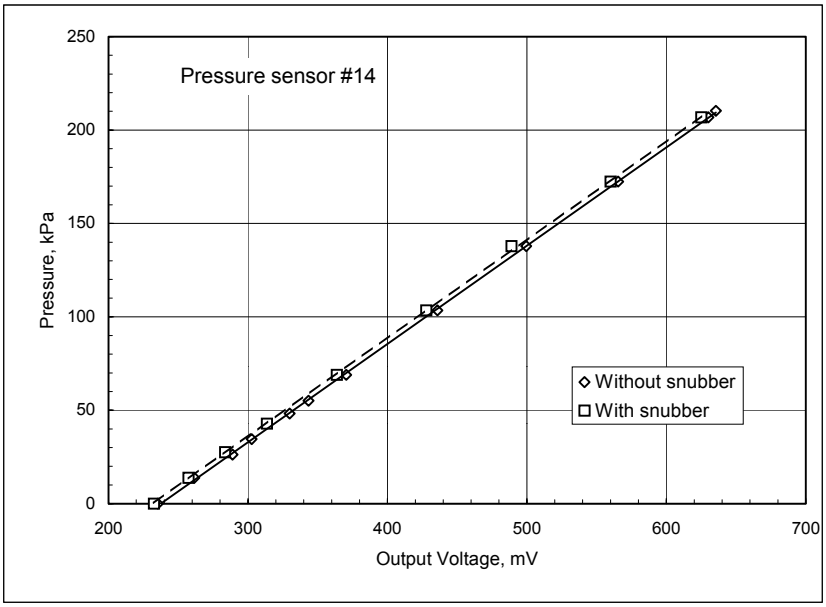

Figure 13. Calibration of pressure sensor (#14) with and without snubber.

Table 1. Calibration coefficients for pressure sensors.

Sensor Number	α, kPa/mV	β, kPa
1	0.7415	88.822
2	0.6756	112.54
3	0.5639	124.33
4	0.5665	158.37
5	0.6704	153.31
6	0.6810	127.79
7	0.5070	97.275
8	0.5047	130.87
9	0.6638	125.93
10	0.6627	155.14
11	0.6723	164.98
12	0.6581	146.89
13	0.5073	120.21
14	0.5264	125.07

One would assume that during the mold filling process coated-sand depositions in the vent areas would cause the vent permeability to decrease. In our previous studies the variation of the pressure losses with the amount of sand+binders depositions in vent area was experimentally measured (Bakhtiyarov and Overfelt, 1998b). In this study we modified the test section to obtain more precise and consistent data for the test sand+binders system. An experimental set up shown in Figures 14 and 15, consists of PVC round tube with an internal diameter D = 19 mm and a length of L = 428 mm. A test vent was installed at the end of the tube. Compressed, dried and pre-filtered air under pressure up to 500 kPa was provided to the tube filled by the test material. The airflow rate was electronically controlled through proportioning valve (ECPV) and controller CN 8511-F1. Rotameters were used to measure the airflow rate. The locations of the pressure sensors along the test tube are presented in Figure 16.

Figure 14. Experimental technique to study pressure losses in core box due to sand deposition in vent area during mold filling process.

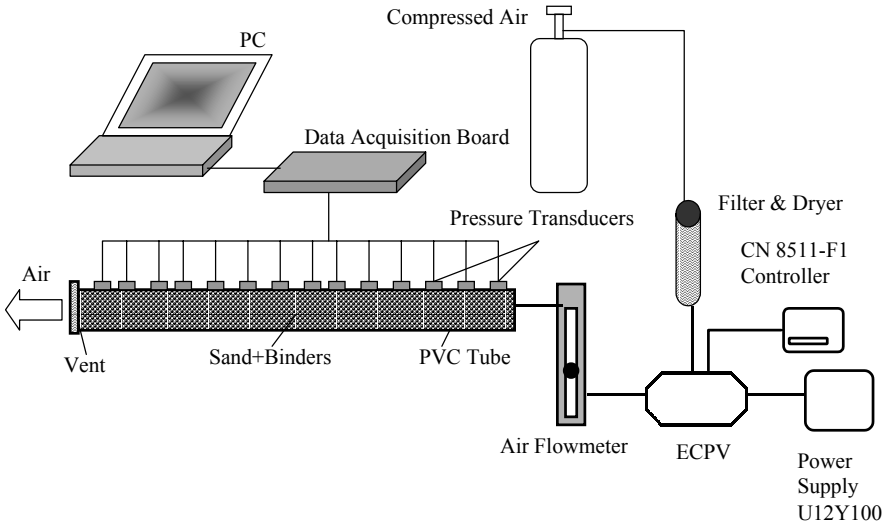

Figure 15. Schematics of experimental technique to study pressure losses in core box due to sand deposition in vent area during mold filling process.

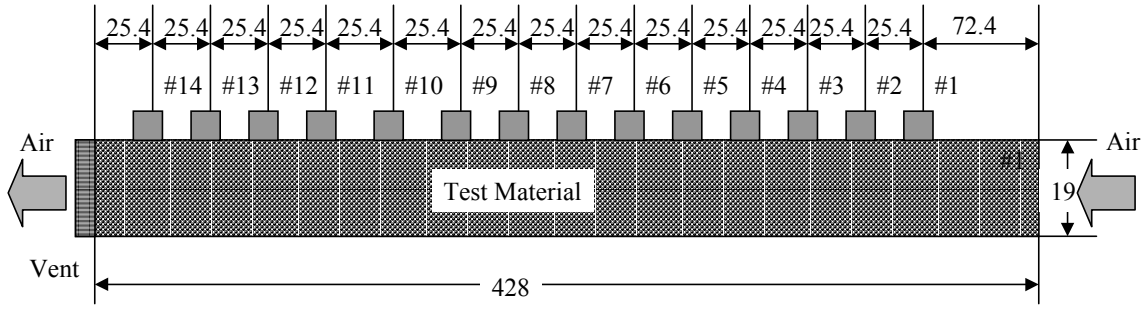

Figure 16. Positions of pressure sensors along the test tube.

The total pressure drop ΔP due to air flow in the cylindrical tube filled by sand (bonded or unbonded) with the vent at the outlet can be represented as,

$$\Delta P = \Delta P_t + \Delta P_v + \Delta P_s, \qquad \text{Equation 12}$$

where ΔP_t , ΔP_v and ΔP_s are the pressure losses in the tube, in the vent and in the sand, respectively. We performed special experiments to estimate the pressure losses due to the tube walls and vent.

The pressure variations against air flowrate in cylindrical tube filled with resin-bonded sand are presented in Figure 17. To simulate the actual sand core-blowing process, sand was not preliminarily compacted in the test tube. Therefore a non-linear relationship between pressure and air flowrate was established. Due to the sand compaction, the pressure increased with increasing the air flowrate for resin-bonded sands. It is shown that the pressure drop increases non-linearly with amount of deposited resin bonded sand in tube. Moreover, at certain values of the air flowrate (~ 250 cm^3/s) a significant increase in pressure drop was observed for resin-bonded sand. We suggest that this behavior is related to the complex rheological behavior of the resin-bonded sand (Bakhtiyarov and Overfelt, 1998b). It was demonstrated, that the resin binders provide some "plasticity" to the sand. The plasticity of the sand+binders mixture is characterized by a shear yield stress, which will provide some resistance to the system against compaction. However, further investigations and analyses are needed to quantify this behavior more precisely.

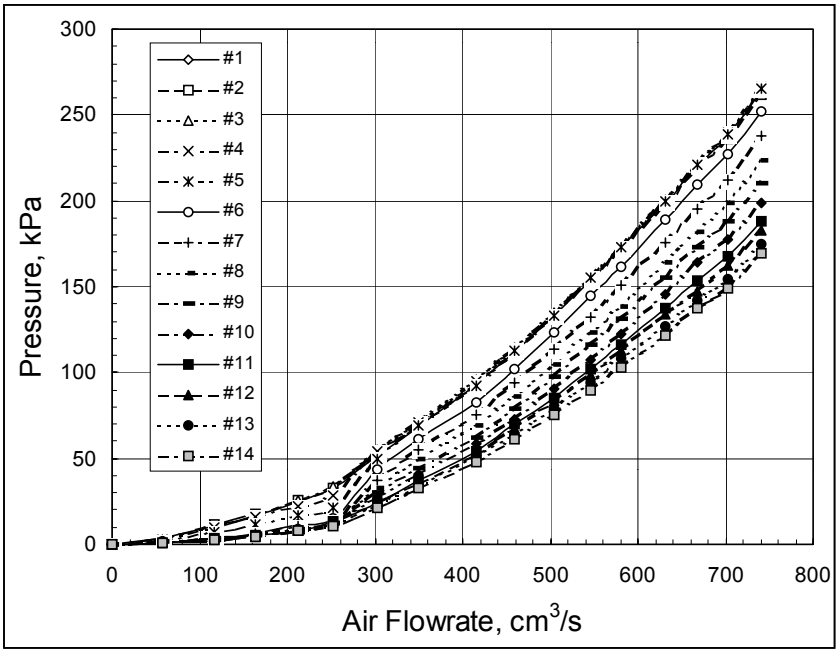

Figure 17. Variation of pressure with air flowrate through resin coated sand.

The flow dynamics of sand and sand-binder system in core box were evaluated in the system shown schematically in Figures 18 and 19. The test core specimens were produced using core-shooting machine. This machine consists of a column, a

shooting unit, a table, fixed and moveable side clamps, a gas carriage, a cabin and a control unit. The machine also houses the control box, the valve manifold and the gas generator. The machine table moves pneumatically under the shooting unit for shooting a sand-binder mixture. When the table has moved down, the gassing plate moves in pneumatically and is pressed between the shoot head and core box when the table has moved up again. Then gassing of the core is started. The gas generator heats liquid catalyst until it reaches a gaseous form. The liquid is dosed (0.2 cm^3/stroke) into a heater where the catalyst evaporates to gas, which is fed to the sand core through a system of gassing plates. The gas together with heated air is blown through the core to purge it. When gassing is complete, the table moves down again, the gassing plate moves out and when the side clamps and cabin doors have opened, the core can be removed from the machine. All functions of the machine are pneumatically moved and controlled. An exhaust system with an exhaust capacity ~500 m^3/h was provided to the cabin. The shape and size (in millimeters) of the core box are shown in Figure 6. The core boxes consisted of the aluminum pattern with clear Plexiglas plate mounted on the front wall to perform visual observations of the flow. The sealing of the core box is achieved when the table is lifted and pressed, creating very strong closing forces on the tooling.

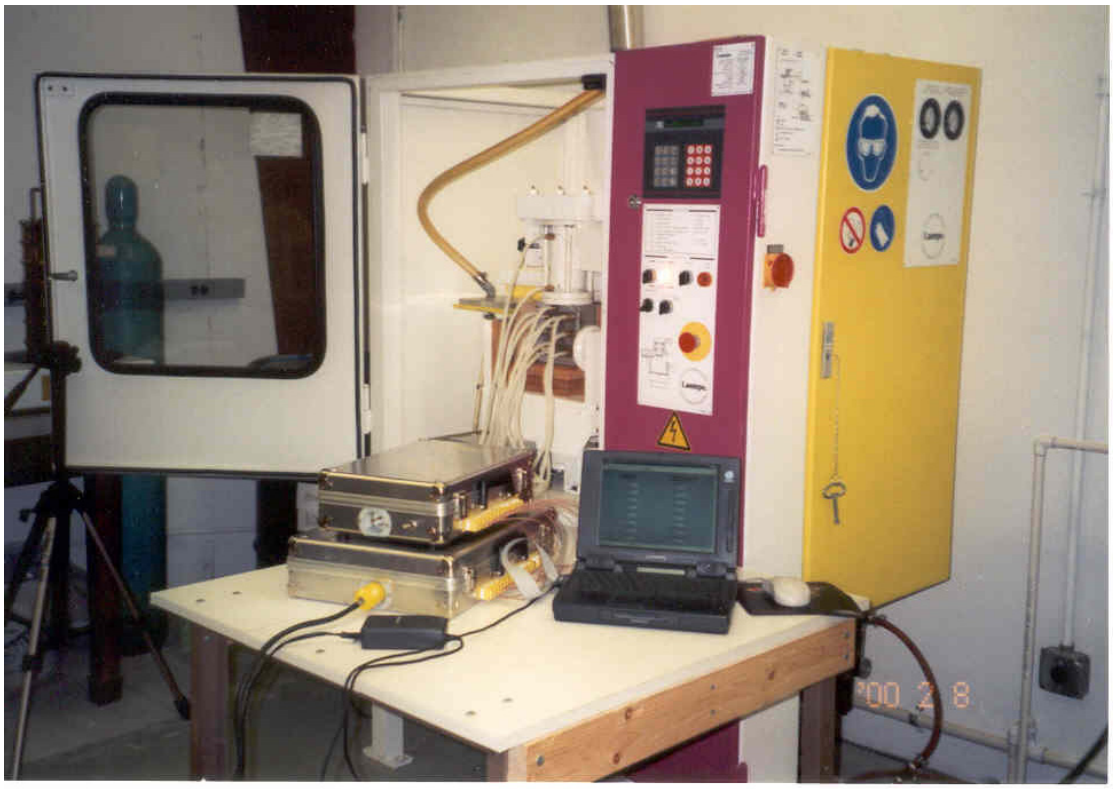

Figure 18. Experimental apparatus used to study dynamics of core shooting process.

In the cold box process, the type, number, size and placement of vents are important factors for core quality, core density and catalyst consumption. They affect the ability to blow a dense and uniform core, and uniform permeation of catalyst gas throughout the core. Recommended total vent area in the cope side is 356 x 10^{-5} to 569 x 10^{-5} cm^2 per gram of core (Carey and Sturtz, 1977). In our experiments we used four slotted steel vents of 12.7 mm diameter and two slotted steel vents of 10 mm diameter with 0.5 mm slots. To evaluate the vent area available to the flow we introduced the mean hydraulic radius R_h, which is the ratio of the cross sectional area of vent available to the flow to the wetted perimeter. Regarding the vent as an opening with a complicated cross section we run experiments to determine the mean hydraulic radius R_h of vent used. A special experimental apparatus was designed and used to determine the hydraulic radius of vents. An average velocity was defined by the Hagen - Poiseuille equation:

$$\langle v \rangle = \frac{\Delta P \, R^2}{4 \, \mu \, L} \, . \qquad \text{Equation 13}$$

The mean hydraulic radius of the vent was defined in terms of the average flow rate and the average velocity in the tube as,

$$R_h = \left(\frac{Q}{\pi \langle v \rangle} \right)^{0.5} . \qquad \text{Equation 14}$$

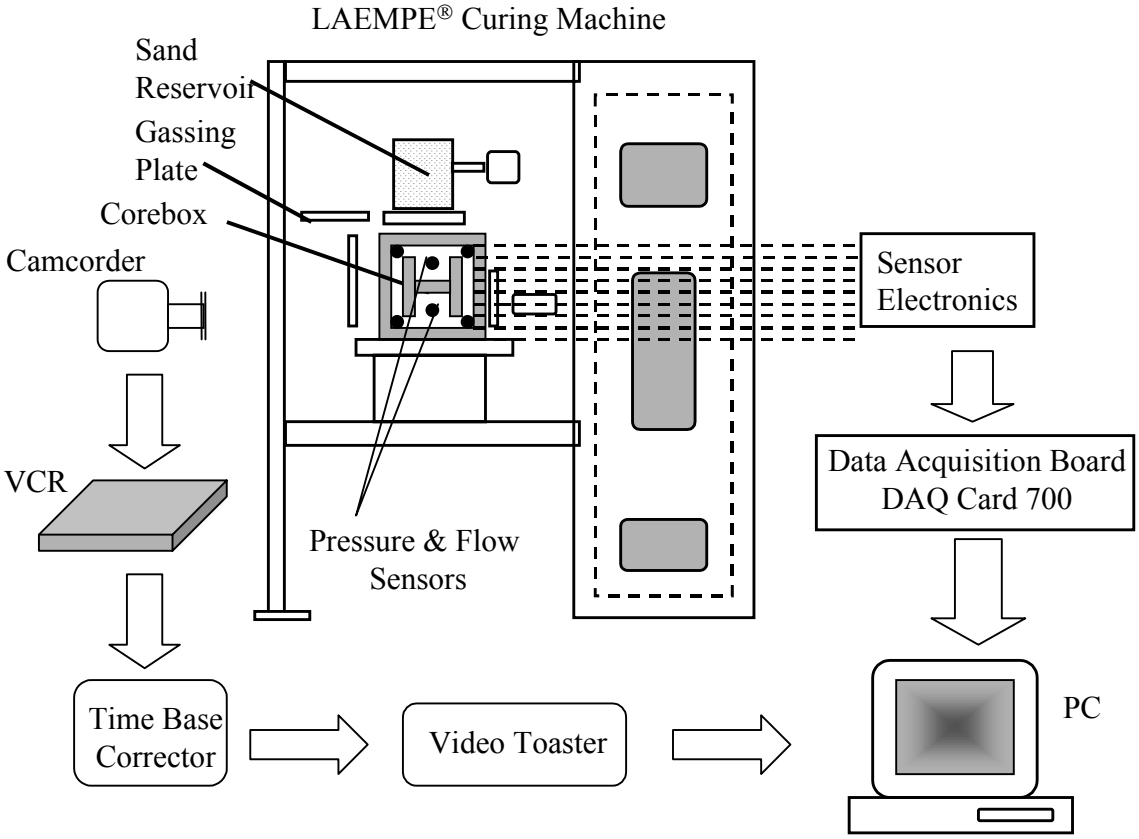

Figure 19. Schematic diagram of experimental apparatus used to study dynamics of core shooting process.

The experimental data suggest that the hydraulic radii of the vents tested are 4.26 mm and 3.35 mm, respectively for vents 12.7 mm and 10 mm in diameter. Hence the hydraulic cross-section areas of the vents are 0.57 cm^2 and 0.35 cm^2, respectively. We present in Figure 20 the number and locations of the vents in the core box. Following the recommendations of Carey and Sturtz (1977) we placed vents in low pockets and near sharp corners so as to direct the sand and the gas catalyst vapors toward those points. During the experiments the total vent area was 3.88×10^{-3} cm^2 per gram of core for core box. The total area of box exhaust vents was 365 % of the total vent input area. The size and shape of the coupling between the hopper and the corebox (input vent) are presented in Figure 21. No special blowtubes were used in these experiments.

Visual observations of the dynamics of the sand blowing process were made by using a video camera recorder (Figure 19). The sand filling patterns and interface displacements were computerized by means of TBC (Time Base Corrector), VT (Video Toaster) and PC "AMIGA". Fourteen piezoresistive absolute pressure sensors were used to measure the pressure variations during the sand blowing and gassing/purging processes in the hopper, blowtube area and in the corebox. The locations of the pressure taps were chosen based on the visual observations of the sand+binders/air flow dynamics (Figures 22 and 23).

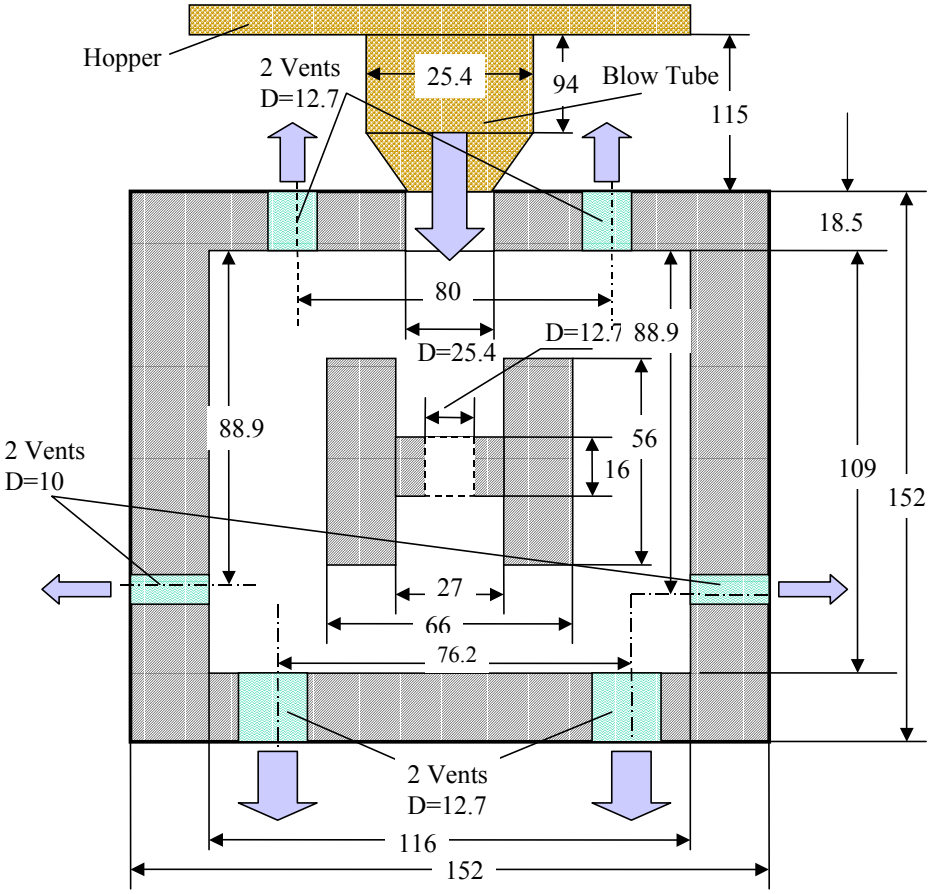

Figure 20. Dimensions of the core box.

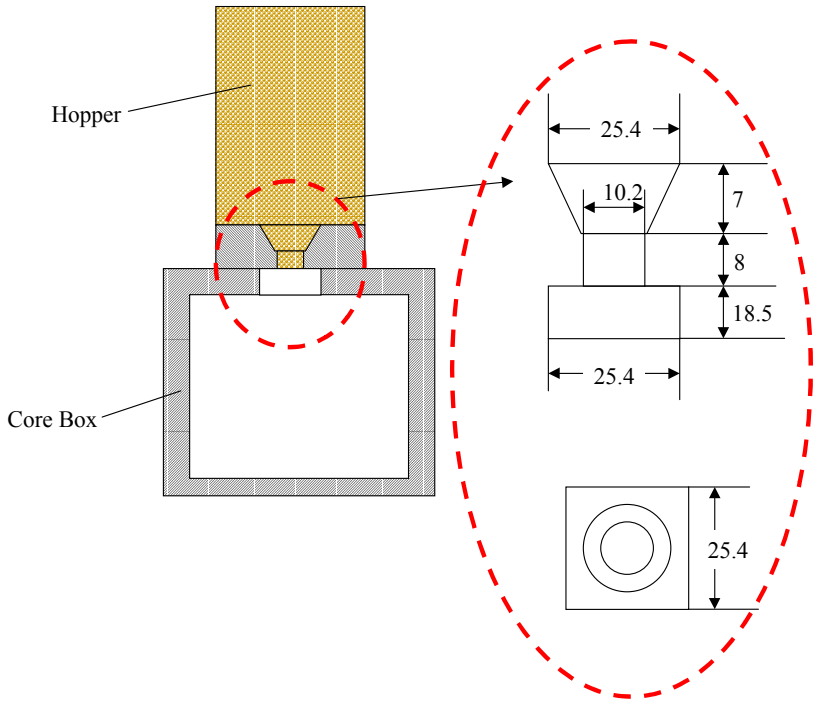

Figure 21. The coupling between hopper and core box.

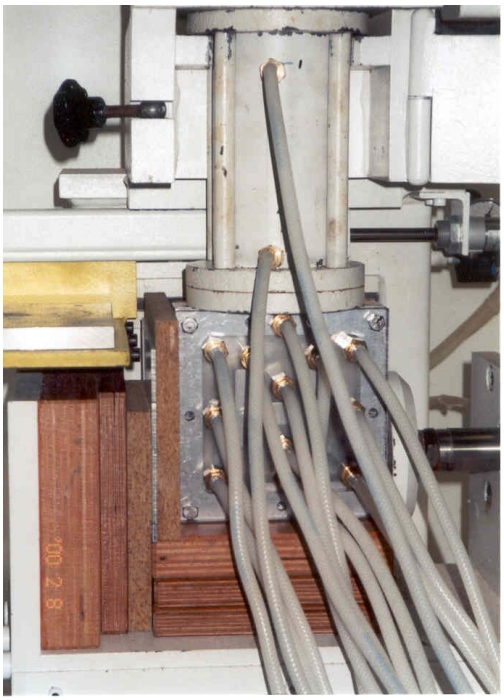

Figure 22. Positions of pressure transducers over the core box.

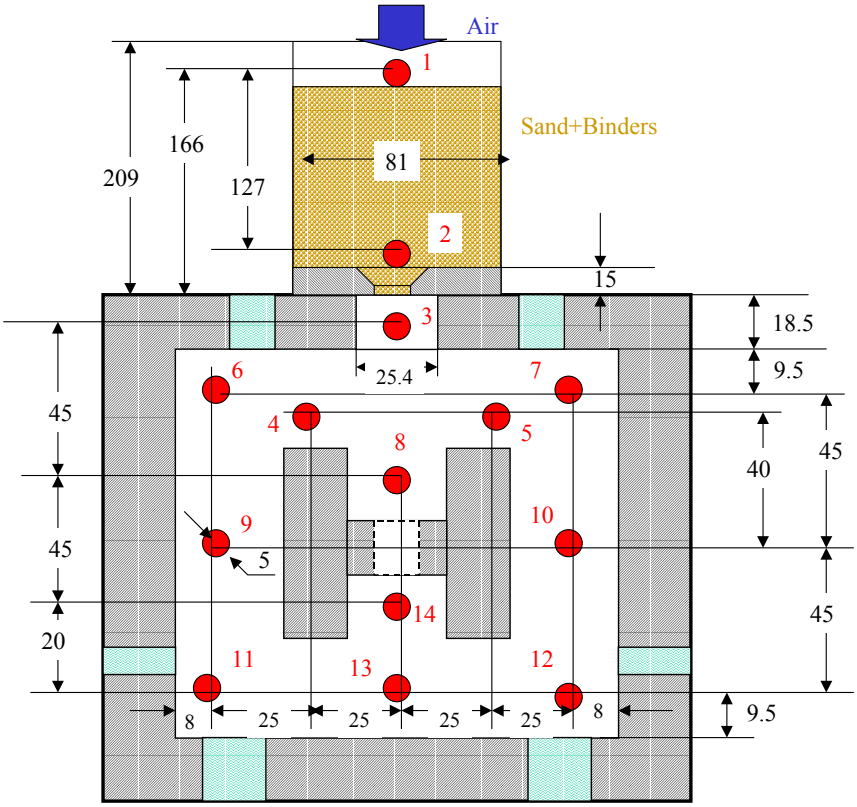

Figure 23. Positions of pressure transducers over the core box.

RESULTS AND DISCUSSION

A variation of pressure (in hopper, blow tube and core box) versus time during sand+binders blowing into the corebox is presented in Figures 24 and 25. As seen from these figures, actual sand shooting takes only 0.2 s. There is a significant difference in pressure values measured in the hopper and in the blowtube area. Due to the large difference in cross section areas of hopper and a blowtube (cross section area of hopper is ten times greater than that of blowtube), we observed a significant decrease of pressure in blowtube. However a pressure decrease also related to the density and sand/air ratio of the resin bonded sand bed. The density of the sand bed in the hopper was 1.426 g/cm^3, and the void factor was $\phi = 0.42$. A vigorous fluidization occurs at the exit from the blowtube. Our previous experiments showed a dramatic decrease in density of the sand bed and increase of the void factor. As we know, fluidized systems require much less energy for through gas flow than the same energy required in case of porous medium. As further fluidization takes place inside the corebox, more decrease in pressure is observed. Sand/air system flow experiences 20 times increase in cross section area, and one would expect a pressure rise in the corebox. However, further fluidization of sand bed happens in the corebox, which decreases density and sand/air ratio of the system. As seen from Figure 25, the pressure inside the core box is twice less than the pressure in the blowtube. The pressure data obtained in these experiments are very informative. From these data one could estimate the variation of the density and the void factor inside the corebox during sand molding process.

The data obtained by barometric measurements were used to create contour maps of the pressure distribution. The isobars were simulated using "cell-valued discretisation" method. The method was described earlier by Bakhtiyarov et al. (1978). This technique has been used earlier to study the dynamics of the displacement of fluids from channels with cavities. Figure 26 presents a pressure distribution (isobars) at the instant of sand shooting inside the corebox. As seen from this figure, a high pressure is found in the area adjacent to the blowtube. The low pressures zones are created at the bottom of the corebox, and under the H-shape insertion of the corebox. Unfortunately, the limited number of pressure transducers prevented creating isobars in small increments of the pressure, and especially revealing stagnation zones inside the corebox. Further experiments are needed to obtain more information on pressure variations during sand mold filling process.

In figure 27 we present the results of both simulations and experiments for pressure variations along the vertical symmetry line of corebox. Here, y is a vertical axis with origin at pressure tap # 3, and H is the distance between pressure taps # 3 and # 13. As seen from this figure, there is good agreement between numerically simulated and measured values of pressure. A significant pressure decrease occurs between blowtube and upper surface of the horizontal section of the insertion. Under the lower surface of this section we can see a parabolic variation of the pressure. Zero values of the pressure refer to the solid surfaces of core box and insertion.

It is of practical interest to identify the pressure distribution inside the corebox during gassing and purging cycles. While during sand mold filling we had a highly fluidized sand/air system, in the gassing and purging cycles air flows through a fixed sand bed. The pressure inside the corebox is mainly affected by properties of the porous medium. Figures 28 and 29 show a variation of pressure (in hopper, blow tube and core box) versus time during air flow through sand+binders bed in coreboxes. Again, a significant pressure drop can be observed in blowtube and inside the corebox. However, pressure segregation across the corebox is more pronounced. The high pressure (~ 25 kPa) is found in the upper portion of the corebox, lowest pressures (~4 kPa) are measured in its lower sections. In contrast to the sand mold filling cycle, as no further significant sand compaction occurred during gassing and purging cycles, we did not observed any peaks on the "pressure-time" curves obtained in blowtube and inside the corebox.

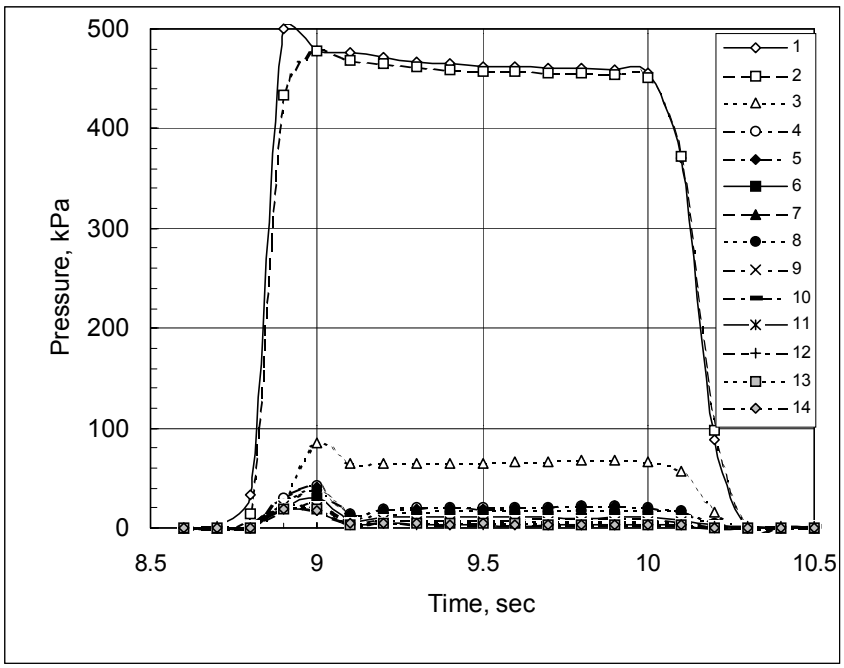

Figure 24. Variation of pressure versus time during sand+binders blowing into corebox (curves 1 and 2 pertain to hopper, 3 to blow tube, and 4-14 to corebox).

CONCLUSIONS

Special experiments were conducted to measure the variation of the pressure with the length of resin bonded sand bed. A non-linear relationship between pressure and air flowrate was established. Due to the sand compaction, the pressure increased with increasing the air flowrate for resin-bonded sands. It is shown that the pressure drop also increases non-linearly with amount of deposited resin bonded sand in tube. Moreover, at certain values of the air flowrate (~ 250 cm^3/s) a significant increase in pressure drop was observed for resin-bonded sand, which is attributed to the complex rheological behavior of the test material. The plasticity of the sand+binders mixture is characterized by a shear yield stress, which provides some "resistance" to the system against compaction. However, further investigations and analyses are needed to precisely quantify this pressure drop behavior.

A significant difference in pressure values was observed in the hopper, blowtube, and inside the corebox, which is related to the cross section area changes and transition of the system from the packed bed to fluidized bed position. The contour maps of the pressure distributions inside the corebox were created based on barometric measurements. A high pressure is found in the area adjacent to the blowtube. The low pressures zones are created at the bottom of the corebox, and under the H-shape insertion of the corebox. A good agreement was found between numerically simulated and measured values of pressure along vertical symmetry axis of the corebox, and actual mold filling time.

A variation of pressure (in hopper, blow tube and core box) versus time during air flow through sand+binders bed in coreboxes (gassing and purging cycles) was studied experimentally. A significant pressure drop was observed in blowtube and inside the corebox. However, pressure segregation across the corebox is more pronounced. The high pressure (~ 24 kPa) is found in the upper portion of the corebox, lowest pressures (~5 kPa) are measured in its lower sections. In the contrast to the sand mold filling cycle, as no further significant sand compaction occurred during gassing and purging cycles, we did not observed any peaks on the "pressure-time" curves obtained in blowtube and inside the corebox.

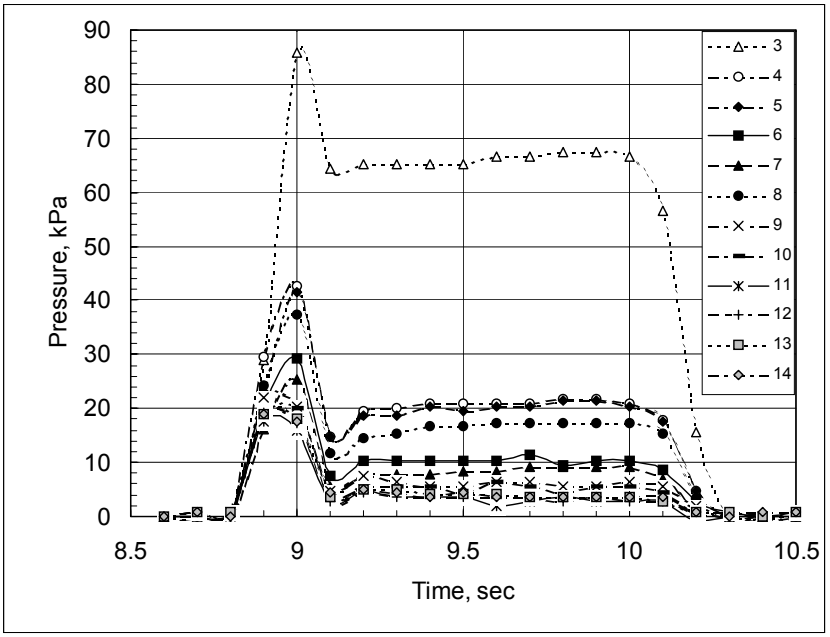

Figure 25. Variation of pressure versus time during sand+binders blowing into corebox (curve 3 pertains to blow tube, 4-14 to corebox).

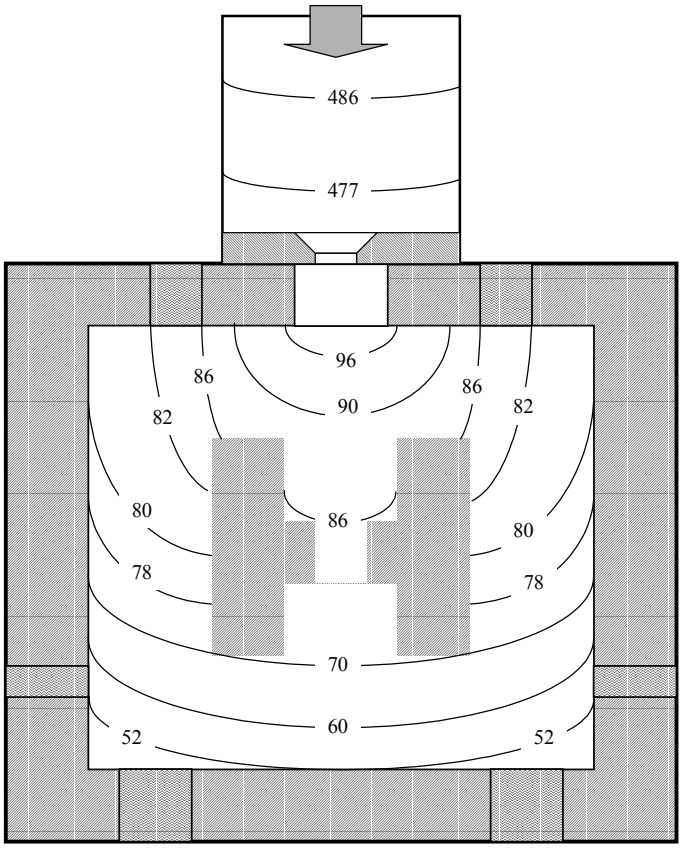

Figure 26. Pressure distribution inside corebox.

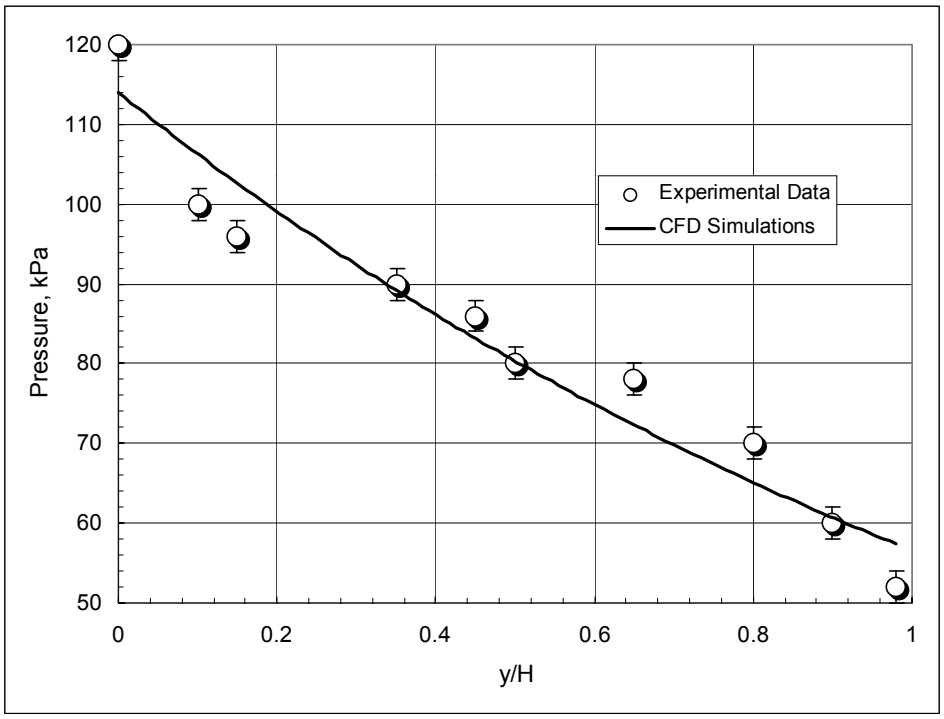

Figure 27. Pressure variations in central vertical line of corebox during mold filling.

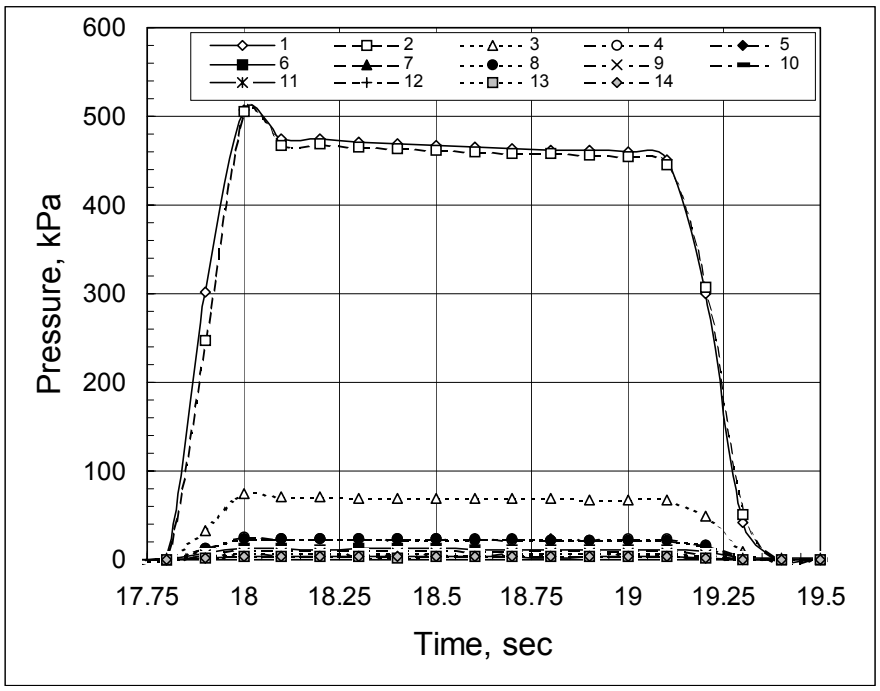

Figure 28. Variation of pressure versus time during air flow through sand+binders in corebox (curves 1 and 2 pertain to hopper, 3 to blow tube, and 4-14 to corebox).

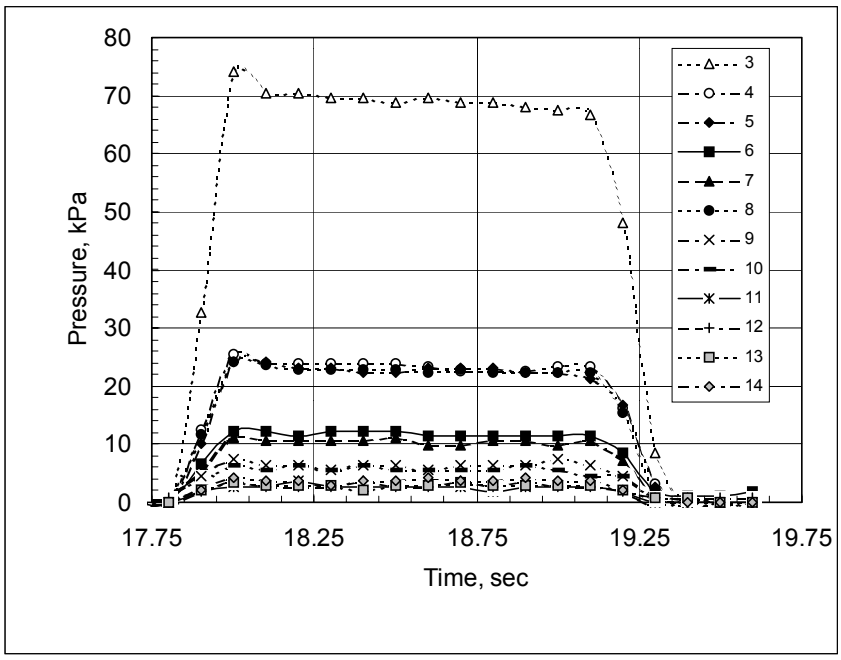

Figure 29. Variation of pressure versus time during airflow through sand+binders in corebox (curve 3 pertain to blow tube, 4-14 to corebox).

ACKNOWLEDGMENTS

The authors wish to acknowledge the financial support received from NASA's Space Product Development at Marshall Space Flight Center under Cooperative Agreement No. NCC8-128. We wish to thank GM Powertrain for supplying samples of Nugent sand and ISOCURE LF-305/904G system. We gratefully recognize the technical assistance of Donald Sirois, Mike Crumpler and John Marcell. Finally, discussions with David Goettsch, Sheila Palczewski, Mike Walker and John Siak of General Motors Corporation on the problems of the phenolic urethane amine cold box process were particularly helpful.

REFERENCES

Ashland Chemical, Inc., "ISOCURE® LF-305/904G", *Foundry Products Division*, No. 1, pp. 1-3 (1994)

Bakhtiyarov, S. I., Overfelt, R. A., Reddy S., "Study of the Apparent Viscosity of Fluidized Sand", Proceedings: Rheology and Fluid Mechanics of Nonlinear Materials - 1996, AMD-Vol. 217, ASME International Mechanical Engineering Congress and Exposition, D. A. Siginer and S. G. Advani, ed., United Engineering Center, New York, N. Y., pp. 243-249 (1996)

Bakhtiyarov, S. I., Overfelt, R. A., "Rheological and Thermal Properties of Phenolic Resin and Polymeric Isocyanate and Their Blends", Proceedings, ASME International Mechanical Engineering Congress and Exposition, Rheology and Fluid Mechanics of Nonlinear Materials, S. G. Advani and D. A. Siginer, ed., ASME United Engineering Center, Dallas, TX, FED-Vol. 243/MD-Vol. 78, pp. 73-77 (1997a)

Bakhtiyarov, S. I., Overfelt, R. A., "Study of Rheological Properties of ISOCURE® LF-305/904G Binder System", *Journal of Elastomers and Plastics*, Vol. 29,No. 4, pp. 314-325 (1997b)

Bakhtiyarov, S. I., Overfelt, R. A., "Rheological and Thermal Characteristics of Technikure® Binder System Used in Core-Box Process", *Journal of Elastomers and Plastics*, Vol. 30, No. 4, pp. 328-339 (1998a)

Bakhtiyarov, S. I., Overfelt, R. A., "Rheological Study of Phenolic-Urethane-Amine Process", *Journal of Elastomers and Plastics*, Vol. 30, No. 1, pp. 11-27 (1998b)

Bakhtiyarov, S. I., Overfelt, R. A., "Experimental and Numerical Study of Sand Core Molding Process", AFS Transactions, vol. 01-049, pp. 1-15 (2001)

Bakhtiyarov S. I., Popov V. I., Khabakhpasheva E. M., "Fluid Displacement from Cavity by Spacer Fluid", *Journal of Oil and Gas*, No. 9, pp. 17-20 (1978)

Bird, R. B., Stewart, W. E., Lightfood, E. N., *Transport Phenomena*, Wiley, New York (1960)

Carey, P. R., Sturtz, G. P., "Updating Resin Binder Processes", *Foundry Management and Technology*, January, pp. 1-7 (1977)

Hoyt, D., "Back to the Basics of Silica Sand", *Modern Casting*, September, pp. 1-4 (1987)

Leva, M., *Fluidization*, McGraw-Hill Book Company, Inc., NY (1959)